6p

19951081 13
324751

N95-14527

ONSET OF HEXAGONS IN SURFACE-TENSION-DRIVEN BENARD CONVECTION*

Michael F. Schatz**, Stephen J. VanHook, J. B. Swift,
W. D. McCormick, and Harry L. Swinney
Center for Nonlinear Dynamics and Department of Physics
The University of Texas at Austin
Austin, TX 78712

ABSTRACT

High resolution laboratory experiments with large aspect ratio are being conducted for thin fluid layers heated from below and bounded from above by a free surface. The fluid depths are chosen sufficiently small (< 0.06 cm) so that surface tension is the dominant driving mechanism; the Rayleigh number is less than 5 for the results reported here. Shadowgraph visualization reveals that the primary instability leading to hexagons is slightly hysteretic (~1%). Preliminary measurements of the convection amplitude using infrared imaging are also presented.

INTRODUCTION

Bénard's landmark experiment [1], which revealed striking hexagonal patterns that arise spontaneously in fluid heated from below, inspired the scientific study of convection and stimulated theoretical ideas ranging from classical hydrodynamic stability to modern notions of pattern formation and complexity in nature. More pertinently, surface-tension-driven Bénard convection (also referred to as Bénard-Marangoni convection) has been recognized as an important paradigm in low-gravity fluid dynamics since it represents a simple, clean example of capillarity-driven flows, which are dominant in the microgravity environment.

Despite its long-standing significance and current relevance, many fundamental questions about Bénard-Marangoni convection remain unanswered. Discrepancies between theory and experiment exist for the primary instability [2]. Secondary instabilities and the transition to turbulence have never been explored. The surface-tension-driven Bénard problem is poorly understood because in terrestrial experiments the effect of buoyancy is often comparable to that of surface tension. Only in space can instabilities and the transition to turbulence in Bénard-Marangoni convection be studied without influence from buoyancy effects. However, in terrestrial experiments on sufficiently thin layers, the effect of buoyancy is negligible at the onset of the primary instability. Such experiments can characterize the primary instability and serve as a basis for studies in space of higher instabilities. Finally, many of the experimental techniques developed and refined for Bénard-Marangoni convection will be directly applicable to other capillarity-driven flows.

In the following, we present results for the onset of convective motion in the Bénard-Marangoni problem. We compare our experimental observations qualitatively to a variational model. In addition, we present preliminary measurements of the temperature field at the fluid-air interface to illustrate the promise of infrared (IR) imaging as a means of obtaining quantitative flow amplitudes.

EXPERIMENTAL

Convection Cell. – The simplest geometry for Bénard-Marangoni convection is the system with a single liquid layer of thickness d_f and horizontal extent $2\Gamma d_f$ bounded at $z = 0$ by a solid surface of high thermal conductivity (1 cm thick aluminum mirror) and at $z = d_f$ by a gas layer of

negligible viscosity and density (Fig. 1). The thickness of the gas layer d_a in the experiments is fixed ($\approx d_f$) by bounding above with a solid surface of high thermal conductivity (1 mm thick sapphire window). A temperature gradient is imposed by heating the mirror to a temperature T_b and by cooling the sapphire window at a temperature T_t. Initially, the surface tension $\sigma(T)$ is uniform at the liquid-gas interface; however, if $T_b - T_t$ is sufficiently large, instability causes surface tension gradients that drive flow along the interface and in the bulk. The dimensionless number that characterizes the surface tension driving is the Marangoni number $M = \sigma_t d_f \Delta T_f / \rho \nu \kappa$, with the liquid density ρ, the liquid kinematic viscosity ν, the liquid thermal diffusivity κ, $\sigma_t = |d\sigma/dT|$, and $\Delta T_f = (T_b - T_t)(1 + k_f d_a / k_a d_f)^{-1}$ in terms of the thermal conductivities k_f and k_a. For any terrestrial experiment, the onset of convection will also depend on buoyancy, which is characterized by the Rayleigh number $R = g\alpha \Delta T_f d_f^3 / \nu\kappa$ with the acceleration of gravity g and the temperature coefficient of volumetric expansion α. The importance of surface tension relative to buoyancy in Bénard-Marangoni convection is given by $\Psi \equiv M/R$; buoyancy effects are negligible when $\Psi >> 1$.

The experiment is performed in a cylindrical cell of diameter $2\Gamma d_f = 3.81$ cm with $d_f = 0.045 \pm 0.0006$ cm and $d_a = 0.050 \pm 0.001$ cm. The thickness of both the fluid and the air layers varies by approximately $\pm$ 1 μm, as measured inteferometrically. Purified dimethylsiloxane silicone oil (96.7% --tetracosamethyldodecasiloxane) is used in the experiment to reduce the potential for subtle thermal cross-diffusive effects that can occur with polymer mixtures such as commercial silicone oils [3]. The heater power to the mirror is computer controlled; with constant heater power, the temperature of the bottom plate fluctuates by less than ±0.0005 °C. The mean temperature of the sapphire window is held constant at 13.32 °C and regulated to ± 0.005 °C. The fundamental time scale in the experiment is set by the vertical diffusion time, $t_v = d_f^2/\kappa \approx 2.2$ s. For the present choice of geometry and working fluid, we have $\Psi = 33$; thus surface-tension effects clearly dominate buoyancy.

Imaging. – The behavior of patterns in Bénard-Marangoni convection is investigated by noninvasive optical methods. The shadowgraph technique is used to detect the onset of convection and to visualize pattern morphology. The shadowgraph images are digitized and enhanced to improve the signal-to-noise using standard image processing techniques. Additionally, infrared (IR) imaging techniques yield the temperature field at the fluid-air interface. The IR imager used in this study is the Amber Engineering Series 5256 ProView system, an LN2 cooled, indium antimonide staring array of size 256 × 256 pixels that operates in the MWIR band from 1.0 to 5.0 μm. To obtain maximum temperature sensitivity and accuracy, multiple data images (typically ~ 64) are acquired at 20 Hz and averaged; an equal number of images of a temperature controlled reference are subsequently averaged and subtracted. To insure that temperature measurements are not averaged over the bulk, a working fluid is used that is composed of methylhydropolysiloxane (30 cS viscosity) mixed with 10 cS Dow Corning 200 silicone oil in a 1:1 ratio by volume. As a result the extinction length for the detected infrared radiation (4.61 micron center wavelength with a bandpass width of 80 nm) is approximately 10 μm.

RESULTS

Hysteresis at Onset–The conduction state undergoes an abrupt transition to hexagons as ΔT_f is increased slowly (average rate $t_v dM/dt = 10^{-6}$). Just prior to onset, a weak circular conduction roll of diameter $\approx d_f$ arises near the boundary; this roll is believed to be driven by static forcing due to the slight mismatch of thermal conductivity between the sidewall and the fluid. Hexagons first appear in a localized section of this conduction roll (Fig. 2(a)). For a given experimental setup, this arc of cells always appears in the same section of the convection apparatus. With a single step increase of 0.15 in M, additional hexagons nucleate from the sidewall and propagate as a traveling front, invading the apparatus until the entire flow domain is filled with hexagons (Fig. 2(b)). The resulting hexagonal planform is free from defects since the lattice is grown from a single "seed crystal" of cells at the boundary. The front of hexagons

propagates across the apparatus in approximately 600 t_v, a time short compared to the *horizontal* diffusion time 4 $\Gamma^2 t_v \approx 7000\ t_v$. The critical Marangoni number is $M_c = 78 \pm 4$ with the uncertainty in the accuracy due to the uncertainty in d_f, d_a, and fluid properties. This compares well with $M_c = 80$ determined from linear stability calculations [4].

On decreasing ΔT_f quasistatically, hexagons continue to persist even as M is reduced to values below that for the first appearance of cells (Fig. 3 (a)-(d)). The hexagons begin to disappear first in regions of the apparatus where they appeared last at onset; thus, the front between convection and conduction propagates in a time-reversed way as compared to onset. However, several steps of size 0.15 in M are required before convection ceases. Moreover, if ΔT_f is held constant before the hexagons completely disappear from the apparatus, the remaining patch of cells persist; in Fig. 3 (c), for example, the patch of hexagons was observed to persist for more than 7000 t_v whereupon continued decrements in temperature caused a return to conduction (Fig. 3 (d)).

Theoretical Model–Near onset, the hexagonal planform arises from the interaction of three roll (plane wave) solutions, k_i, k_j, k_k, each of which has a magnitude equal to the critical wavenumber and makes an angle of $2\pi/3$ with the other roll solutions [5]. Under these conditions, the evolution of the planform is described the set of (real) amplitude equations of the form:

$$d_t A_i = \varepsilon A_i + \alpha A_j A_k - A_i(A_i^2 + \gamma(A_j^2 + A_k^2)) \qquad (1)$$

where the indices are cyclically permuted. Under certain assumptions, the coefficients can be computed from the full fluid equations [6, 7]. The existence of hexagons requires $\alpha \neq 0$; as a result, the bifurcation from the conduction state is *subcritical,* i.e., it occurs discontinuously like a first order phase transition. With $\varepsilon = (M/M_c - 1)$, the solutions for hexagons and for conduction are linearly stable over a range of parameter: $\varepsilon_\alpha < \varepsilon < 0$ with $\varepsilon_\alpha = -\alpha^2/(2+4\gamma)$ (the conduction state is linearly unstable for $M > M_c$).

The amplitude equations form a variational model; such a system is expected to exhibit relaxational time dependence governed by a potential function V [8]. Over the range of parameter where both conduction and hexagons exist, each solution corresponds to a minimum of V, where one solution represents the global minimum of V while the other solution, the metastable phase, represents a local minimum. However, there exists a parameter value ε_m (often called the Maxwell point) where both solutions have equal values of the potential; as the parameter value passes through ε_m, the solutions exchange the roles of global stability/metastability. For Eqs. (1), the conduction state is globally stable for $\varepsilon < \varepsilon_m = -8/9\ \varepsilon_\alpha$ and metastable for $\varepsilon_m < \varepsilon < 0$.

The experimental observations are consistent with this variational model. The conduction state enters a metastable regime $\varepsilon > \varepsilon_m$ as ΔT_f increases. The hexagons that first appear at the boundary provide a sufficient perturbation to push the system over the potential barrier and the front between the two states propagates in a way such that the globally stable state (hexagons) spreads. When ΔT_f is decreased, hexagons become metastable for $\varepsilon < \varepsilon_m$. Since the range of parameter values where hexagons are metastable is nearly an order of magnitude smaller than the region of metastability for conduction, the transition back to conduction will be more sensitive to small spatial variations in ε due to nonuniformities in the depths of both the fluid and air layers. As a result, the transition back to conduction occurs in stages, with the front halting as soon as the local value of ε is equal to ε_m.

Surface Temperature Measurements–Local amplitude measurements are necessary to provide direct, quantitative comparison to theoretical models (such as Eqs. (1)) and to numerical simulations. Toward this end, high-resolution infrared imaging is being investigated; Figure 4 illustrates a preliminary measurement of surface temperature near onset. A spatially varying ε is intentionally imposed by increasing the surface temperature (hence, decreasing ΔT_f) from left to

right in Fig. 4; the interface between conduction and convection is quite sharp, in qualitative agreement with the shadowgraph images in Fig. 3. This measurement demonstrates that the temperature resolution, which is better than 0.1 °C, is sufficient to examine quantitatively the behavior of Bénard-Marangoni convection near onset.

CONCLUSIONS

The experimental observations of an abrupt onset of convection and hysteretic return to the conduction state support the idea that the primary instability in Bénard-Marangoni convection is subcritical; further quantitative investigation is being conducted to characterize the degree of subcriticality. One outstanding question is the determination of the range in ε over which hysteresis occurs. Our initial measurements indicate that this range may depend on the size and rate at which the temperature (and, hence, ε) is stepped. Such behavior is not surprising since subcritical transitions may be triggered by finite amplitude perturbations (temperature fluctuations, nonuniformity at the boundary); it remains to be seen to what extent such perturbations may be reduced in our experiments. Additionally, we are developing more quantitative measures of experimental geometry and fluid properties to determine more accurately the critical Marangoni number M_c and are conducting extensive measurements of surface temperature near onset using infrared imaging.

*Work supported by the NASA Microgravity Science and Applications Division Grant NAG3-1382.
**Author to whom correspondence should be directed--email: schatz@chaos.utexas.edu.

REFERENCES

1. Bénard, H., Rev. Gen. Sci. Pure Appl., 1 (1900), 1261.

2. Koschmieder, E. L. and Biggerstaff, M. I., J. Fluid Mech., 167 (1986), 49.

3. Moses, E. and Steinberg, V., Phys. Rev. Lett., 57 (1986), 2018.

4. Pearson, J. R. A., J. Fluid Mech., 4 (1958), 489.

5. Ciliberto, S., Coullet, P., Lega, J., Pampaloni, E. and Perez-Garcia, C., Phys. Rev. Lett., 65 (1990), 2370.

6. Davis, S. H., Annual Review of Fluid Mechanics, 19 (1987), 403.

7. Bestehorn, M., Phys. Rev. E, 48 (1993), 3622.

8. Malomed, B. A., Nepomnyashchy, A. A. and Tribelsky, M. I., Phys. Rev. A, 42 (1990), 7244.

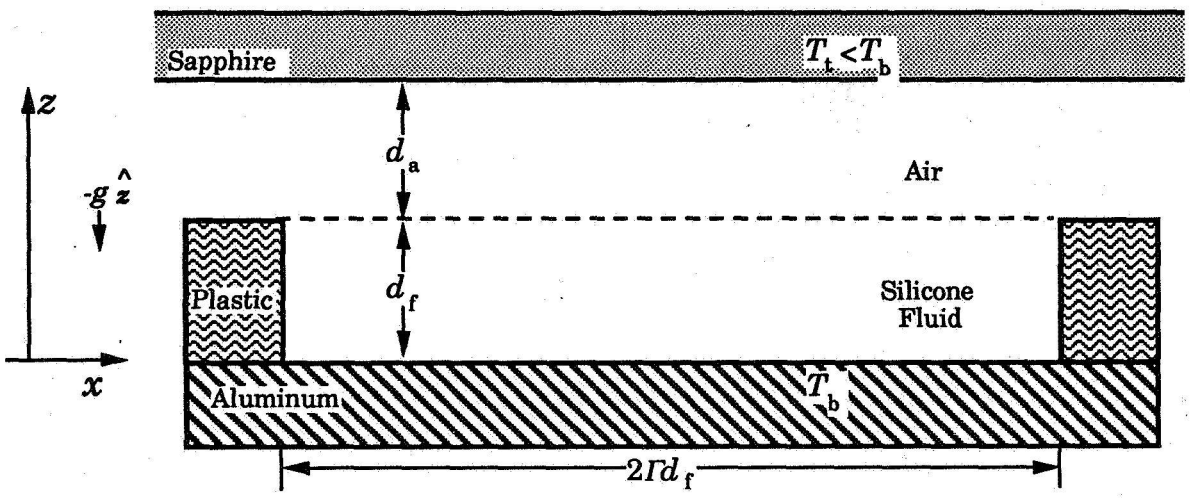

Figure 1: Geometry of Bénard-Marangoni convection

INCREASING M

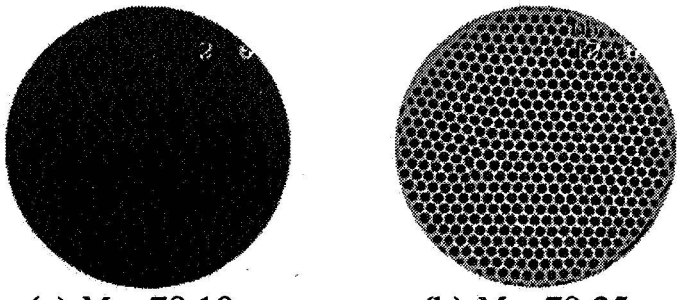

(a) $M = 78.10$ (b) $M = 78.25$

Figure 2: Shadowgraph images depict a sharp onset in surface-tension-driven Bénard convection.

DECREASING M

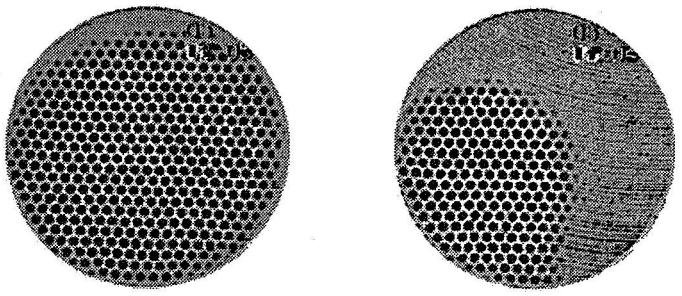

(a) $M = 78.25$ (b) $M = 77.75$

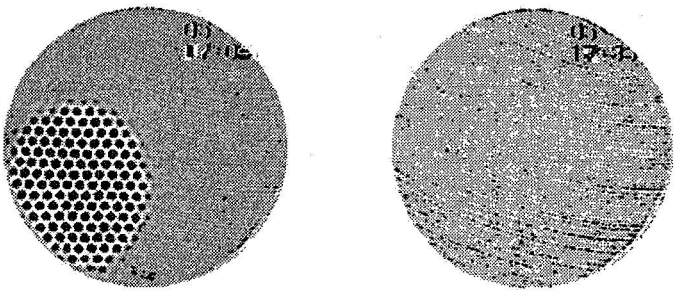

(c) $M = 77.50$ (d) $M = 77.30$

Figure 3: Hexagonal convection persists at values of M below onset, indicating a hysteretic transition (compare to Figure 2).

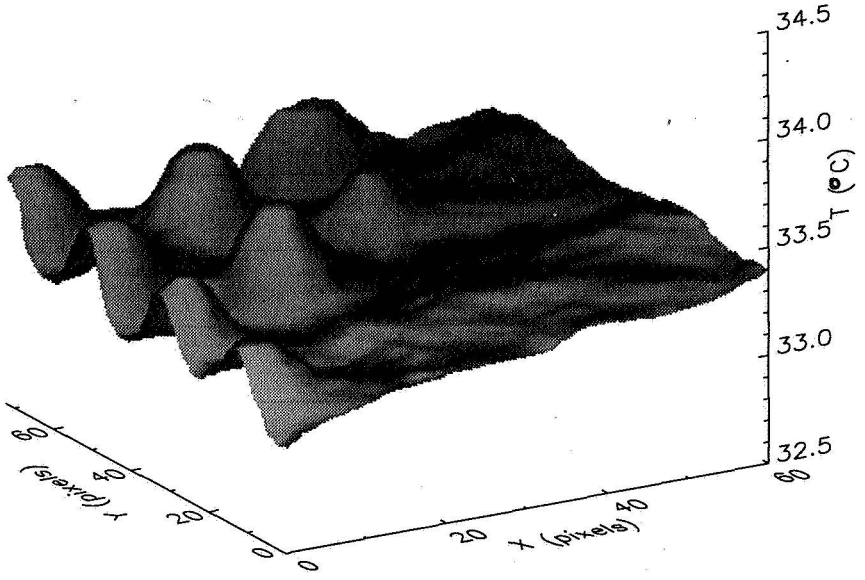

Figure 4: Fluid surface temperature measured near onset by infrared imaging.